

## Seismic and vibration tests for assessing the effectiveness of GFRP for retrofitting masonry structures

Paul Michelis<sup>1</sup>, Costas Papadimitriou\*<sup>2</sup>, Grigoris K. Karaikos<sup>2</sup>,  
Dimitra-Christina Papadioti<sup>2</sup> and Clemente Fuggini<sup>3</sup>

<sup>1</sup>*Institute of Mechanics of Material & Geostuctures S.A., 22 Askiton str., Penteli, 152 36, Greece*

<sup>2</sup>*University of Thessaly, Department of Mechanical Engineering, Volos 38334, Greece*

<sup>3</sup>*D'Appolonia S.p.A., Industrial Innovation Division, Via Martiri di Cefalonia, 2,  
20097 San Donato Milanese (MI), Italy*

(Received October 1, 2011, Revised November 10, 2011, Accepted February 10, 2012)

**Abstract.** Full-scale shake table seismic experiments and low-amplitude vibration tests on a masonry building are carried out to assess its seismic performance as well as study the effectiveness of a new multifunctional textile material for retrofitting masonry structures against earthquakes. The un-reinforced and the retrofitted with glass fiber reinforced polymer (GFRP) strips masonry building was subjected to a series of earthquake excitations of increasing magnitude in order to progressively induce various small, moderate and severe levels of damage to the masonry walls. The performance of the original and retrofitted building states is evaluated. Changes in the dynamic characteristics (lowest four modal frequencies and damping ratios) of the building are used to assess and quantify the damage states of the masonry walls. For this, the dynamic modal characteristics of the structure states after each earthquake event were estimated by performing low-amplitude impulse hammer and sine-sweep forced vibration tests. Comparisons between the modal results calculated using traditional accelerometers and those using Fiber Bragg Grating (FBG) sensors embedded in the reinforcing textile were carried on to investigate the reliability and accuracy of FBG sensors in tracking the dynamic behaviour of the building. The retrofitting actions restored the stiffness characteristics of the reinforced masonry structure to the levels of the original undamaged un-reinforced structure. The results show that despite a similar dynamic behavior identified, corresponding to reduction of the modal frequencies, the un-reinforced masonry building was severely damaged, while the reinforced masonry building was able to withstand, without visual damage, the induced strong seismic excitations. The applied GFRP reinforcement architecture for one storey buildings was experimentally proven reliable for the most severe earthquake accelerations. It was easily placed in a short time and it is a cost effective solution (covering only 20% of the external wall surfaces) when compared to the cost for full wall coverage by GFRPs.

**Keywords:** masonry structures; glass fiber reinforced polymers; shake table tests; structural identification; health monitoring; damage assessment

---

### 1. Introduction

A large number of masonry structures exist in high seismicity regions throughout the world. Most masonry structures have been designed without following design procedures recommended by modern seismic codes. Such structures are vulnerable to damage and collapse due to moderate and

---

\*Corresponding author, Professor, E-mail: [costasp@uth.gr](mailto:costasp@uth.gr)

large earthquakes. Un-reinforced brick masonry buildings perform poorly under (lateral) seismic forces, failing in out-of-plane bending, in-plane bending and shear. Although being the most widely used type of construction in the world it is not capable of dissipating energy through inelastic deformation. They are designed to resist primarily gravity and wind loads.

Retrofitting techniques provide the means of stiffening and strengthening these structures to withstand earthquakes. Several retrofitting strategies have been proposed in the past. Among the retrofitting techniques, repair technologies based on fiber-reinforced polymer (FRP) are effective and practical alternatives for stiffening and strengthening masonry buildings. A large number of tests on the components of the masonry structures have been performed to study the effectiveness of the retrofitting on the component level using pseudo-dynamic shear-compression (Marcari *et al.* 2007, Fam *et al.* 2002), flexural (Liu *et al.* 2007), out-of-plane (Mosallam 2007, Tan *et al.* 2003, Albert *et al.* 2001, Triantafillou 1998), dynamic (Bastianini *et al.* 2005) and seismic shake table (Turek *et al.* 2007) tests. Tests have also been performed to investigate analytically and experimentally the behaviour of masonry beams (Kiss *et al.* 2002a, 2002b) under strengthening with fiber reinforced plastics. Tests on complete masonry structures have also been performed using pseudo-dynamic (Casciati 2010, Agarwal and Thakkar 2004, Paquette *et al.* 2004) and shake table (Wight *et al.* 2007, Benedetti *et al.* 2001) tests under different strengthening and retrofitting actions and the performance of masonry structures has been evaluated under the action of earthquakes. These tests have provided valuable information on the seismic performance of full scale masonry buildings or the components of the masonry.

Reinforcement by FRP (mainly externally bonded carbon or glass fiber reinforced polymer) increases substantially the masonry load capacity, the static bending capability, the ductility and the overall stiffness. The mode of deformation, including the crack pattern on the masonry walls, depends on the wall boundary conditions and reaction zones, which were not real in most of the component test cases examined in the Laboratory. These observations are particularly valid for dynamic (cyclic) loading, in-plane and out-of-plane, developing during earthquakes. Experimental data based on shake table tests and field data from full-scale masonry buildings should be assessed to improve the masonry wall reinforcement design in order to increase the overall stiffness, strength and ductility (energy absorption capability) under real boundary conditions that prevail on full scale structures. The aim of the tests should be to optimize strength and deformability in a synergistic interaction in order the reinforcement to become an integral structural part. The reinforcement design should ensure, through strengthening and deformability, that highly stressed zones are not developing in the reinforced masonry and also in the surrounding un-reinforced masonry and that the building will resist: out-of-plane bending, in-plane bending, in-plane shear, combined with axial load.

The objective of this study is threefold. The first objective is to experimentally investigate through shake table tests the seismic performance of full-scale, single room, un-reinforced masonry buildings and to validate the effectiveness of glass fiber reinforced polymer (GFRP) strips as retrofitting techniques in an effort to improve the masonry wall stiffness, strength and ductility to withstand earthquakes. The second objective is to investigate and monitor the health of the structure through low amplitude dynamic testing and correlate the change in the dynamic characteristics of the structure to the intensity of ground shaking, the damages observed and the retrofitting actions carried out using repair techniques and strengthening with GFRP material bands. Lastly, the third objective is to investigate the feasibility of FBG sensors embedded in the reinforcing textile fabric in detecting and tracking the changes of the dynamic characteristic of

the building in terms of evolution of modal frequencies and damping ratios during the shaking table tests.

The change of the dynamic characteristics, such as modal (resonant) frequencies and modal damping ratios, with damage and strengthening actions on the building are useful damage or strengthening index indicators (Casciati and Al Saleh 2010, Casciati and Hamdaoui 2008, Beni *et al.* 2003) and coupled with finite element models can also be used for vulnerability assessment studies (Casciati and Faravelli 2010). In particular, these damage indicators can be used for evaluating the degree of damage induced under seismic actions and the level of retrofitting steps required in order to restore the stiffness of the structure.

A series of shake table tests followed by low amplitude vibration tests were performed on a masonry building at its un-reinforced and reinforced configurations. The masonry building was designed in full scale to resemble typical brick masonry building types, encountered in the countryside. The un-reinforced masonry building was subjected to a series of progressively intensified earthquakes until it was severely damaged, evident by the large crack openings in the four walls of the building. Then it was repaired, strengthened with GFRP strips until its original stiffness is recovered, and re-tested with a similar second series of progressively intensified earthquakes to evaluate the effectiveness of the reinforcement. An innovative multifunctional (reinforcing plus monitoring functionalities) GFRP textile material, optimally wrapped along the masonry walls following existing guidelines, developed under the European research project POLYTECT ([www.polytect.net](http://www.polytect.net)), is considered as retrofitting solution for un-reinforced masonry structures (Messervey *et al.* 2010). The FBG sensors, embedded in the reinforcing textile material, allow for strain measurements along their length and offers sampling rate up to 1000 Hz, which is feasible for dynamic measurements. Appropriate damage indices based on the observed evolution of the modal frequencies are introduced to monitor the health of the masonry structure and evaluate the effectiveness of retrofitting actions. Three different building and reinforcement configurations have been studied. The present study reports results from the third building and reinforcement configuration which was optimally designed based on existing guidelines and the experience from the tests on the first two masonry structures. The full-scale experimental tests are aimed to improve design retrofitting guidelines for masonry structures, taking into account realistic boundary conditions at the sides of the masonry walls, wall continuity at the corners and wall openings from windows and doors.

This study is organized as follows. Section 2 introduces the masonry building, the geometrical characteristics, the material properties identified from component tests, and the finite element model that was developed based on simplified assumptions on composite brick-mortar wall behavior. Details for the shake table facility and the building instrumentation are provided in Section 3. Section 4 presents the experimental set-up, giving details about the series of seismic experiments performed on the un-reinforced and the reinforced building along with the observed damages during the tests. Section 5 concentrates on the post-earthquake low-amplitude vibration tests performed to trace the evolution of the modal characteristics of the masonry structure under the progressively intensified seismic events and retrofitting actions. It presents and discusses results for the correlation of the identified resonant frequencies and damping ratios with intensity of seismic excitation and stiffness degradations due to damage caused from the applied seismic events, or stiffness restoration resulted from strengthening actions. Attention is also paid to assess the correlation among the results calculated from accelerometers data and those calculated from FBG sensors data. Conclusions are summarized in Section 6.

## 2. Description of masonry building and modeling

### 2.1 Building description with geometry

A full-scale single-story (one-room) brick-masonry building is designed and constructed in the laboratory. The un-reinforced single-room brick building is representative of a portion of the build inventory, particularly in the Greek countryside. The single-room building is used in this study since it simulates actual conditions at the sides of the masonry walls, wall continuity and large wall openings from doors and windows. The geometry of the masonry structure is shown in Fig. 1. The masonry structure consists of four single masonry brick walls with two opposite doors and windows, and a reinforced concrete roof. The four walls of the masonry building are anchored on the shake table using the mortar to assemble the bottom face of the clay bricks of each side wall with the shake table surface. This connection was used to simulate the actual anchoring conditions of common (old) masonry buildings to their foundation. The top view dimensions are 3.19 m parallel to the X-axis and 2.78 m parallel to the Y-axis. The structure height is 2.26 m (including 10 cm concrete roof thickness). The door's width and height is 0.70 m and 1.64 m, respectively and it is placed on the center of the two opposite wall's width. The window's width and height is 0.70 m and 0.70 m, respectively and it is placed on the center of the other two opposite wall's width. The layout of the door and window openings results in a symmetric building, avoiding eccentricities as much as possible. This symmetry was purposely introduced to reduce the number of dominant factors (material, mortar-brick, connections, large openings) that affect building behavior without compromising the value of this study since all other masonry building characteristics are maintained. All the surrounding walls are 8.5 cm thick, determined by the width dimension of the bricks.

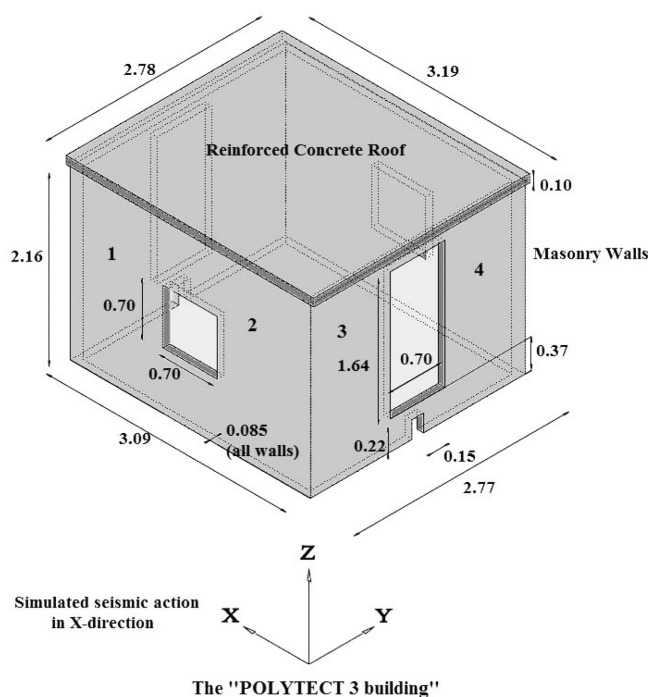


Fig. 1 Geometric of masonry building

## **2.2 Building materials and component tests**

The construction of the masonry wall panels was based on common practices in Greece. The bricks were common bricks often used for the construction of masonry structures. The building brick is a rectangular, hollow multicored, clay prism of long dimension 187 mm (parallel to the holes), height 112 mm (perpendicular to the holes and along the vertical direction) and width 85 mm (perpendicular to the holes and along the horizontal direction), weighting about 1.70 Kg.

Components tests were conducted separately on bricks, mortar and brick-mortar assemblies in order to understand their mechanical behavior and obtain their mechanical properties. These tests were performed using the mechanical testing equipment available on the Institute of Mechanics of Materials and Geostrutures (IMMG). The tests included compression tests along directions parallel and perpendicular to the brick holes, as well as shear tests. In particular, based on the tests carried out on brick-mortar assemblies, consisted of a small number of building bricks bonded by mortar, the constitutive parameters in compression, tension and shear of the brick-mortar panels were experimentally measured. Compression tests on panels with the loading direction parallel to the brick holes confirmed higher peak strength values (nominal value of 4 MPa at 0.4% strain) but lower stiffness in comparison with loading of bricks normal to the holes where a nominal peak strength value of 3 MPa at 0.17% strain was measured. The mortar joint shear strength was found to be 0.7 to 0.75 MPa. Each compression test was repeated for several specimens and a significant variation in the stiffness was observed. For example, the stiffness for the compression test with loading of bricks normal to the holes varied from 2.3 to 3.5 GPa. Similar ranges of variations were observed for the compression tests with loading parallel to the brick holes.

## **2.3 Finite element model of the masonry building**

A detailed finite element (FE) model of the masonry building at its undamaged un-reinforced state was created based on the geometric details and the material properties of the reinforced concrete roof and the masonry walls. The structure was designed in the COMSOL Multiphysics (COMSOL 2005) finite element modelling environment. The finite element model for the structure was created using three-dimensional tetrahedral solid finite elements to model the whole structure. The elements along the basement are fixed in the direction of motion and the same applies for those linking the four walls and the concrete roof. The nominal values of the mechanical properties of the brick-mortar components and the reinforced concrete roof are used to construct a nominal linear finite element model of the masonry structure from the behavior of its components. Based on existing mechanical tests and the low strain levels expected to be experienced by the reinforced concrete roof during low-amplitude vibration tests, the roof was assumed to be homogeneous isotropic with material properties as follows: elasticity modulus  $E=30$  GPa, Poisson ratio  $\nu=0.2$  and density  $\rho=2500$  Kg/m<sup>3</sup>. A homogeneous orthotropic material was assumed for the masonry walls to roughly account for the periodic structure of the brick-mortar elements. Based on the experimentally obtained stress-strain relationships, the following nominal values for the mechanical properties were assumed for the composite brick-mortar units: elasticity modulus parallel to the brick's holes  $E_1=1.8$  GPa, elasticity modulus vertical to the brick's holes  $E_2=2.3$  GPa, shear moduli  $G_1=0.64$  GPa and  $G_2=0.82$  GPa, Poisson ratio  $\nu_1=\nu_2=0.4$  and average density  $\rho=1000$  Kg/m<sup>3</sup>. It consists of 8341 solid finite elements and has 50553 degrees of freedom.

The linear finite element model of the building was constructed as a reference model in order to

understand the dynamic behavior of the building under the various low intensity seismic excitations and get a rough idea of the modal characteristics (modal frequencies and mode shapes) of the building for the purpose of instrumentation and later the correlation between the identified and analytical modes. Furthermore the FE model, as it was conceived and implemented, served for two additional purposes. The first was to identify a preferring location and dimension of the GFRP strips, as a function of the stress field distribution across the masonry walls. The second purpose was to help in identifying a preferable FBG sensors topology (i.e., sensors location and numbers) in order to get useful data during the shaking table tests, to be able to prove the effectiveness of such type of sensors in dynamic measurements.

The model constitutes a simplified modeling of the complex behavior of the composite brick-mortar system. A more accurate modeling based on homogenization theories (Salerno and Felice 2009, Stefanou *et al.* 2008) is expected to yield a much better description of the behavior of the masonry walls. In addition, the reinforcement using GFRP strips introduced extra modeling complications. However, such modeling details are out of the scope of the present study.

### 3. Shake table facility and building instrumentation

#### 3.1 Shake table description

The tests were performed at IMMIG. A unidirectional textile shake table was designed and constructed at IMMIG for carrying out the seismic test campaign. The dimensions of the shaking table are 4 m by 3 m. The table is accelerated using a displacement controlled servo-hydraulic system, developed and validated within the European Research Project “POLYTECT” ([www.polytect.net](http://www.polytect.net)). The table has the following two original characteristics. It is not metallic but textile table, produced by a glass-reinforced honeycomb panel, manufactured by IMMIG based on the patented DIRIS architecture (Directionally Reinforced, Integrated, Stretched, Sing yarn). This panel is light, weighting only 210 Kg and extremely stiff, exhibiting the highest shear strength in in-plane and out-of-plane loading. The actuation-control mechanism of the servovalve is piezoelectric, reacting much faster and more precisely than the ones available in the market. Exploiting the previous capabilities, the shaking table possesses the following characteristics. It is capable of sinusoidal, random, shock and arbitrary time history excitation, it has a maximum payload of 10 Ton, maximum displacement of  $\pm 120$  mm, maximum acceleration of 4 g (with 10 Tons payload), and frequency limit of 100 Hz. The previous technical characteristics classify the facility as one of the few operating in Europe but with one distinction: its very low cost of construction (<10% of the equivalent European facilities) and operation.

#### 3.2 Building instrumentation

As many as twelve (12) uni-axial accelerometers, six (6) piezo beam and six (6) K-beam capacitive accelerometers, were mounted on the shake table and the structure in order to record the severity of the seismic excitation and the vibration levels experienced by the structure along all three directions, as well as to identify the structural modal characteristics from low-amplitude vibration tests. The sensor locations along with the monitoring directions are shown in Fig. 2. The sensor configurations depend on the series of the two tests conducted on the un-reinforced and reinforced masonry building. Only six (6) sensors were placed on the structure as shown in Fig.

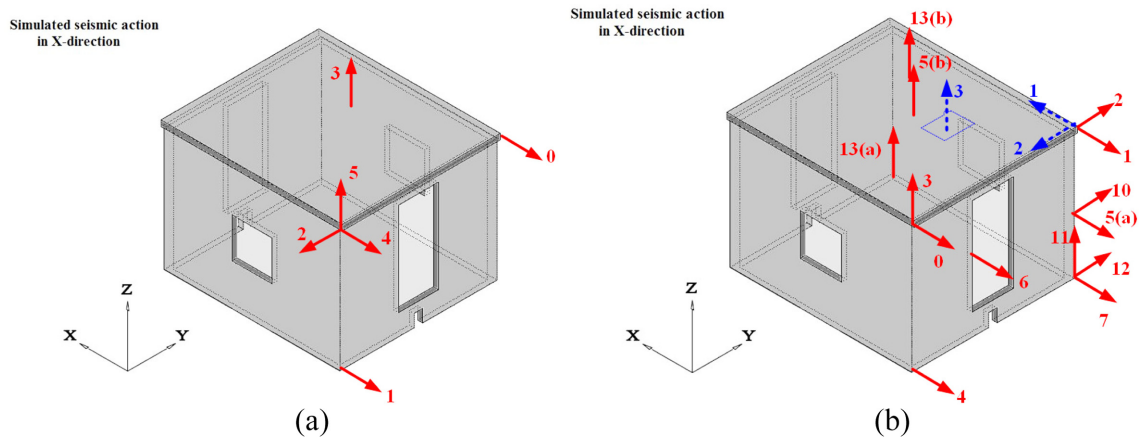


Fig. 2 Sensor configurations (solid arrows) and hammer impact points (blue-broken arrows) on the masonry structure, (a) un-reinforced building and (b) reinforced building

2(a) during the series of tests conducted for the un-reinforced masonry structure. Twelve (12) sensors were placed on the structure as shown in Fig. 2(b) during the series of tests conducted for the reinforced masonry structure. For the reinforced structure, three different sensor configurations were employed based on the series of tests conducted and the experience gained from previous tests on similar reinforced masonry structures.

In general, up to as many as five sensor locations on the base of the reinforced structure were activated during the tests in order to monitor the acceleration of the shake table in all directions. Two of the acceleration positions (sensors 4 and 7) measure the horizontal base acceleration along the  $x$ -direction of the motion of the shake table. One sensor (sensor 12) measures along the horizontal  $y$ -direction perpendicular to the direction of motion and two sensors (sensors 11 and 13a) measure along the vertical  $z$ -direction in order to check possible rocking effects during the motion of the shake table.

A group of sensors was placed at the roof level to monitor the global motion of the masonry unit, and another group was placed at approximately the mid-height of the front wall to monitor in-plane and out-of-plane vibrations of the wall. A set of sensors was also placed on the roof to monitor the vibrations along its vertical direction and the out-of-plane motion of the roof. The sensor location was carefully designed so that all the response of the structure during the excitations from the earthquakes imposed by the shake table is carefully monitored and the important low frequency modes are identified during the low amplitude forced vibration tests performed after each seismic event. Experience from previous tests performed on the laboratory for two very similar structures were also used to guide the design of the sensor locations and directions.

In addition to the accelerometers sensors, during the shaking table tests of the reinforced building, 8 FBG sensors from the Light Structures company (Norway) were installed in key positions, with the configuration shown in Fig. 3(a). Their topology was designed based on some preliminary FEM results and on the crack patterns as assessed after the last seismic test of the un-reinforced building (see Fig. 3(b)). The recorded strain time histories are subsequently analysed in the frequency domain for estimating the structural modal characteristics and investigating their reliability and accuracy compared to conventional methods based on processing acceleration time history signals.

With reference to Fig. 3(a), it is worth noting that the active length of the FBG sensors varied

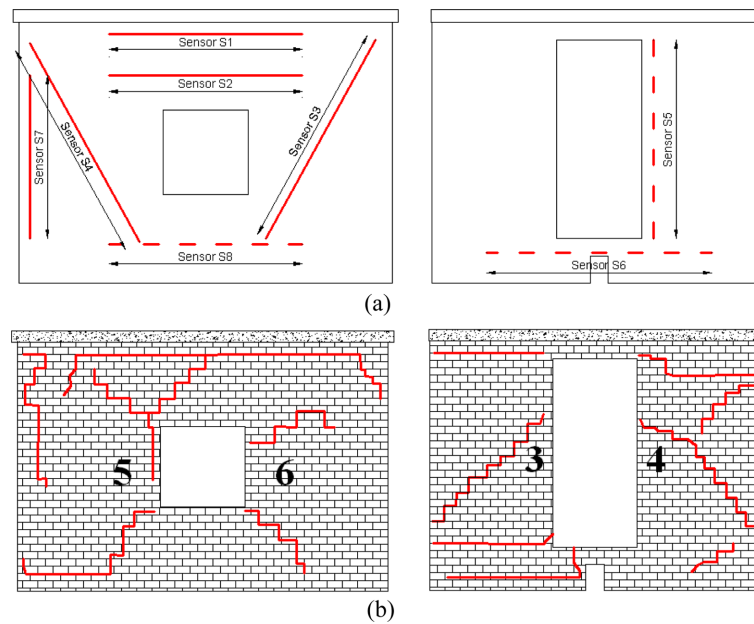


Fig. 3 (a) FBG Sensor configurations for the reinforced building and (b) schematic diagram of crack patterns of the two walls depicted in Fig. 6(a) after the last shaking table test of the un-reinforced building

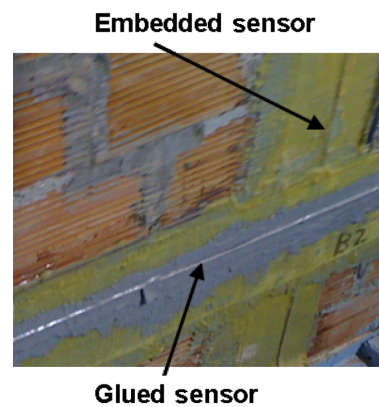


Fig. 4 Detail on FBG sensors glued and embedded on the reinforced building

from 1 to 1.5 m, according to the prediction of the strain-stress field distribution as calculated from FE models. The continuous lines in Fig. 3(a) represent sensors which were externally glued to the textile (due to the absence of cables embedded into the textile in the chosen location), while the dashed lines sensors represent sensors which were embedded into the FRP. A picture of the detail for glued and embedded strain sensors is shown in Fig. 4.

#### 4. Shake table seismic experiments and damage results

The objectives of the experiments are threefold. The first objective is to study the seismic



performance of the un-reinforced masonry building and to evaluate the effectiveness of GFRP strips for retrofitting the structure to withstand earthquakes. The second objective is to investigate the change in the dynamic characteristics (modal frequencies and damping ratios) of the structure in terms of the intensity of ground shaking and correlate this change with the intensity of the shaking and the damage observed. Lastly, the third objective is to prove the feasibility of FBG sensors in detecting the building dynamics in terms of evolution of modal frequencies and damping ratio during the shaking table tests.

The un-reinforced masonry building was subjected to a series of progressively intensified earthquake events until it was severely damaged, evident by the large crack openings in the four walls of the building. Then it was repaired, strengthened with GFRP strips and re-tested using a second series of progressively intensified seismic events. The objective of the seismic experiments is to investigate the vulnerability of the un-reinforced building and then investigate the effectiveness of the GFRP reinforcement on the masonry building to withstand the second series of seismic events.

Section 4.1 describes the series of shake table tests performed on the un-reinforced masonry structure and reports the damages induced in terms of crack formation and openings in the masonry walls. Section 4.2 describes the repair procedure for the damaged masonry structure followed by the reinforcement of the masonry walls by GFRP strips. The results of second series of shake table tests performed on the retrofitted structure are presented in Section 4.3. The correlation of damage with the dynamic characteristics of the masonry structure during the various excitation phases is presented in Section 5.

#### *4.1 Shake table tests of the un-reinforced masonry building*

The seismic excitations exerted by the shake table were generated by scaling the intensity and the time of an artificial accelerogram, compatible with the elastic spectrum provided by the European Code EC8 for acceleration level  $a_g=0,15$  g. The artificial accelerogram is shown in Fig. 5(a). The displacement time history obtained by double integration of the artificial acceleration is fed as a command signal to the shake table facility in order to be reproduced at the shake table base. Fig. 5(b) compares the corresponding command displacement time history fed to the shake table with the real displacement time history (shifted along vertical axis to facilitate comparison) actually induced and measured at the shake table. A very good agreement between the command displacement signal and the real displacement time history induced at the shake table is observed which confirms the effectiveness of the shake table facility.

A series of six (6) seismic excitation events were conducted that correspond to various peak ground acceleration (PGA) values selected to represent various levels of seismic intensity. These intensity levels were accomplished at the shake table by either scaling the intensity of the command displacement in the table, or scaling the time over which the earthquake was applied, or a combination of intensity and time scaling. The time scale instead of the intensity scale in the displacement time history was introduced in order to exert progressively higher intensity seismic events at the shake table without exceeding the maximum displacement constraints for the particular shake table facility. Table 1 reports the information on the six seismic events, including the corresponding scale in intensity and time, and the actual PGA values recorded by the acceleration sensor placed on the shake table. In addition to the peak ground accelerations (PGA) along the direction of motion, the theoretical PGA values are also reported normalized so that they coincide with the measured PGA values for the un-scaled earthquake excitation. It can be seen that the acceleration at the base has

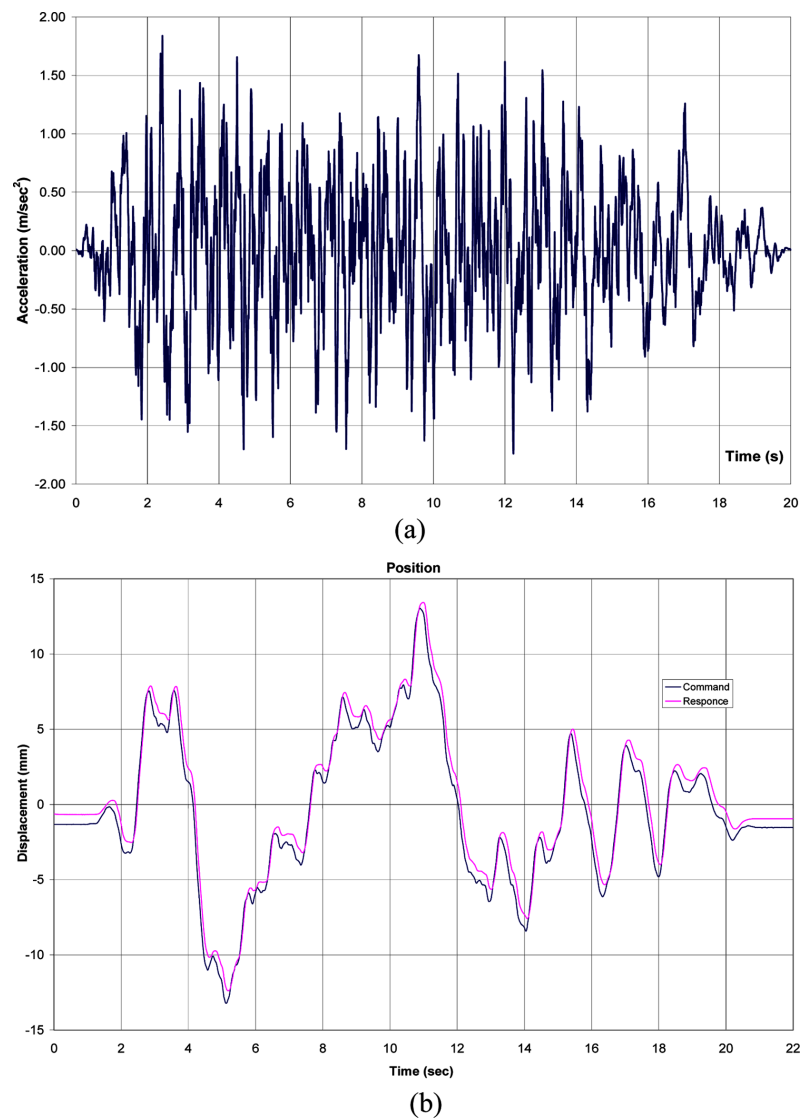


Fig. 5 (a) Artificial earthquake compatible with EC8 elastic spectrum for  $a_g=0.15$  g and (b) comparison between command and recorded displacement time history at the shake table

Table 1 Excitation characteristics of the seismic events applied on the un-reinforced building

Seismic event	Intensity scale (% of European earthquake)	Time scale (sec)	PGA recorder values (g)	PGA theoretical values (g)
1 <sup>st</sup>	20%	20	0.10	0.06
2 <sup>nd</sup>	60%	20	0.29	0.19
3 <sup>rd</sup>	100%	20	0.32	0.32
4 <sup>th</sup>	100%	15	0.52	0.57
5 <sup>th</sup>	100%	10	0.99	1.28
6 <sup>th</sup>	100%	7	2.50	2.56

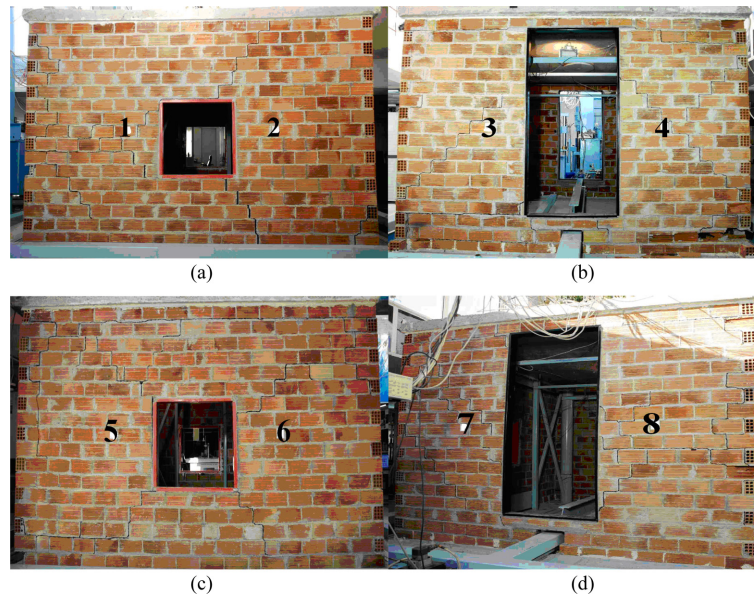


Fig. 6 The sides of the masonry building damaged after the application of the sixth seismic event

exceeded 2.5 g.

The un-reinforced masonry building sustained the first five seismic events without suffering any serious visible damage. The last seismic event, which was theoretically intensified almost 8 times the original seismic event, heavily damaged the building with large crack openings developed along the walls and propagated mainly through the mortar. The four sides of the masonry building after the application of the sixth seismic event are shown in Fig. 6. A schematic diagram of the patterns of the major crack developed on the two sides of the walls that were instrumented by FBG is shown in Fig. 3(b). Based on visual inspection, the sixth seismic event generated shear failure of many bricks and mortar, diagonal cracking on the walls, extensive flexural faults and measurable shear sliding in the walls 1, 2, 5 and 6. Larger crack openings were observed on the two sides of the wall with the window openings that extend along the direction of motion. The other two sides of the building walls, with the door openings that extend along the perpendicular direction of motion, also sustained serious damage. All the walls were damaged but it seems that the in-plane shearing (walls 1-2 and 5-6) produced more damage than the out of plane loading (walls 3-4 and 7-8). Overall, during the action of the sixth seismic event, the masonry building sustained serious visual damage, with the walls losing their structural integrity and posing increased threat to occupants due to high risk of collapse to future seismic excitations.

#### *4.2 Repair of damaged masonry building and reinforcement with GFRP strips*

The heavily damaged masonry building walls were repaired and strengthened. The restoration event refers to retrofitting of the damaged parts and application of an optimally designed GFRP strip reinforcement. Specifically, for retrofitting the damaged parts, the concrete roof was lifted, the cracked mortar and broken bricks along all four side walls of the building were removed and new mortar and bricks were placed. At the end the roof was bonded on the brick walls, as previously.



Fig. 7 A picture of the repaired masonry building with reinforced GFRP strips: (a) sides 1-2 and (b) sides 3-4

The walls were carefully examined and small open cracks were cleaned with pressurized air and filled with pressurized epoxy in order to repair the structure and provide the necessary continuity between the different components.

The repairing design consists also of external reinforcement by bonding peripherically, tensioned glass fibre thermoplastic strips, with spacing in agreement with the CNR-DT/2004 guidelines (CNR-DT 200/2004). Specifically, after the repair work was completed, the masonry walls were reinforced by GFRP strips against out-of-plane and in-plane loading, according to the CNR-DT/2004 guide. The results from FE analyses were also used as guidance for placing the GFRP strips. Fig. 7 show the GFRP strip reinforcement along the masonry building walls 1-2 and 3-4. Exactly the same reinforcement patterns were applied along the masonry building walls 5-6 and 7-8. The GFRP strips are 150 mm wide, 3 mm thick and have 4 kN tensile strength.

The GFRP strips were bonded on the bricks, initially by polymer and then by polymer-cement plaster of B.G. Polymers company from Israel. The patterns – positioning of the strips were designed to maximize the out-of-plane resistance for the walls with the doors (sides 3, 4, 7 and 8) and the in-plane resistance to shear for the walls with the windows (sides 1, 2, 5 and 6) along the direction of loading. To this end the strips are parallel in the walls with the doors and diagonal in the remaining walls with windows. The thin and flexible strips allow the masonry to move (to micro-slide) and therefore to mobilize more effectively reaction mechanisms to absorb energy. Also the symmetry of the strip layout prevents eccentric stiffness and strengthening that may cause twisting.

The driving objective for the GFRP reinforcement was to create, through externally bonded GFRP strips, a flexible connection between the walls, the roof and the floor of the building in order to obtain a 3D – reaction to external loading :

- by confining the orthogonal walls with tensioned GFRP horizontal strips, which surround the building at the top and bottom of the walls. Then, tensile strength is transferred to the walls against out-of-plane and in-plane loading. In this way, the reinforced zones at the top and bottom behave like reinforced – masonry beams.
- by bonding vertical and/or diagonal strips, anchored under the previous horizontal strips.

This combination of strips develops a stereo-reinforcement, where the parts of the assembly are strained in synergy under different conditions (compressive, tensile, shear-torsion). Peak loading is reduced and energy absorption is maximized.

It should be noted that the retrofitting actions are expected to partly restore the stiffness of the structure. The degree of stiffness restoration will be examined in Section 5. The existence of the GPFR reinforcement provides the reinforced structure with ductility and higher capability of absorbing energy at low strains.

### 4.3 Shake table tests of masonry building repaired and reinforced with GFRP strips

A new series of earthquake excitation tests were conducted on the retrofitted building by scaling the intensity and time of the 2009 L' Aquila W-E earthquake accelerogram, shown in Fig. 8. This particular record from the destructive L' Aquila earthquake event was made available after the test campaign on the un-reinforced masonry building. It is more representative of the strong motion expected in parts of the Mediterranean region as opposed to the ground motions predicted by the artificial accelerogram shown in Fig. 5(a). For the purpose of our present study that concentrates on damage evaluation based on the dynamic characteristics of un-reinforced and reinforced masonry, the use of the L' Aquila record does not qualitatively influence the respective results and conclusions. Thirteen (13) seismic excitation events were included in the new series of tests. The thirteen excitations correspond to various intensity levels of the L' Aquila earthquake. As before, the different intensity levels were accomplished at the shake table by either changing the intensity of the command displacement in the table or scaling the time over which the earthquake was applied. Table 2 reports the information on the thirteen seismic excitation events, including the corresponding scale in intensity and time. It also gives the recorded and theoretical PGA values along the direction of motion.

In contrast to the severe damage observed for the un-reinforced building at the end of the sixth seismic event, no damage was observed in terms of visible cracks on the mortar, the bricks or the interfaces between them. The integrity of the masonry walls, seeing as a unit of bricks and mortar, and the integrity at the interface between the masonry walls and the table or the roof, was preserved. Comparing the characteristics of the two series of shake table seismic tests applied on the un-reinforced and reinforced building in Tables 1 and 2, respectively, it is obvious that in the case of the reinforced building, higher peak ground accelerations are recorded. Specifically, the last earthquake applied on the reinforced building has a ground shaking with PGA almost two times the PGA of the base shaking for the sixth earthquake applied on the un-reinforced building. Despite this stronger shaking of the reinforced building, the reinforced masonry performed very well and withstood the

Table 2 Excitation characteristics of the seismic events applied on the reinforced building

Seismic event	Intensity scale (% L' Aquila earthquake)	Time scale (sec)	PGA recorded values (g)	PGA theoretical values (g)
1 <sup>st</sup>	20%	20	0.15	0.07
2 <sup>nd</sup>	60%	20	0.29	0.21
3 <sup>rd</sup>	100%	20	0.35	0.35
4 <sup>th</sup>	100%	15	0.41	0.62
5 <sup>th</sup>	100%	12	0.93	0.97
6 <sup>th</sup>	100%	11	0.61	1.15
7 <sup>th</sup>	100%	10	1.16	1.40
8 <sup>th</sup>	100%	9	1.39	1.73
9 <sup>th</sup>	100%	8	1.50	2.19
10 <sup>th</sup>	100%	7	2.90	2.85
11 <sup>th</sup>	100%	6	3.90	3.89
12 <sup>th</sup>	100%	6	3.90	3.89
13 <sup>th</sup>	100%	7	4.00	2.80

very strong ground shaking with no visible damage. It can be concluded that the reinforcement was sufficient to maintain the structural integrity of the masonry walls.

## 5. Damage evaluation based on dynamic characteristics

The health state of the structure after each shake table test was evaluated by monitoring the modal dynamic characteristics such as modal (resonant) frequencies and modal damping ratios. These characteristics were identified by carrying out very low-amplitude forced vibration tests after each seismic event. These low-amplitude vibration tests, described in Section 5.1, are used to measure the modal characteristics and correlate the evolution of these characteristics with the stiffness degradation and observed damage caused by the seismic events. The reduction of the lower modal frequencies of the masonry structure after the application of each earthquake event is used as a damage index (Casciati and Hamdaoui 2008, Beni *et al.* 2003) to provide an overall measure of the damage state of the masonry structure at its un-reinforced and reinforced configurations. The correlation of the modal characteristics with the seismic intensity, building damage induced by seismic actions and strengthening induced by retrofitting actions is reported in Section 5.2. The feasibility of the FBG sensors measurements in the frequency domain to track the variation of the dynamic characteristics is also investigated.

### 5.1 Post-earthquake low amplitude forced vibration tests

The low amplitude vibration tests were performed with a PCB086D20 impulse hammer equipped with a medium tip head in order to excite the important lower modes of the masonry structure needed for the evaluation of its dynamic characteristics, such as modal frequencies, modal damping ratios and mode shapes. The vibration tests were performed before the shaking table tests were initiated and immediately after each earthquake event was inflicted by the shaking table on the structure. The purpose of the impulse hammer tests was to identify the dynamic characteristics of the structure and mainly to trace the change in the modal frequencies and the damping ratios as a function of the severity of the seismic excitation and the observed damage.

After each earthquake event, a total of 6 impulse hammer tests were conducted. The impact force was inflicted along the two horizontal directions and one vertical direction in order to excite all lower important modes of the structure. The impact points and directions are shown in Fig. 2(b) with blue (broken) arrows. Two independent tests per each excitation direction were performed. Each impulse hammer test lasted only a few seconds allowing to speed up considerably the whole procedure of acquiring data from the structure.

The un-reinforced building was instrumented with six (6) sensors shown in Fig. 2(a) for all low amplitude post-seismic vibration tests. During the first four (4) seismic tests (1<sup>st</sup>, 2<sup>nd</sup>, 3<sup>rd</sup>, and 4<sup>th</sup>), the reinforced building was instrumented with 10 accelerometer sensors (sensors 0, 1, 2, 3, 4, 5, 10, 11, 12 and 13 in Fig. 2(b)). During the 5<sup>th</sup>, 6<sup>th</sup> and 7<sup>th</sup> seismic tests the building was instrumented with 12 accelerometers. Acceleration sensors were added at positions 6 and 7 in Fig. 2(b) and the sensors 5(a) and 13(a) in the set up shown in Fig. 2(b) were re-positioned (at locations 5(b) and 13(b) in Fig. 2(b)) on the roof of the building as shown in Fig. 2(b). This sensor relocation was necessary in order to monitor the *z*-direction and take more accurate measurements of the out-of-plane mode of the concrete roof where strong motion was detected. During the final six (6) seismic

events (8<sup>th</sup> to 13<sup>th</sup> events) the building was again instrumented with 12 accelerometers. The location of sensor 13(b) in sensor configuration shown in Fig. 2(b) was changed to its original location 13(a). In addition, for all the 13 tests of the reinforced building, 8 FBG sensors were also installed in the GFRP, having the configuration shown in Fig. 3(a).

To verify the reliability and accuracy of the dynamic characteristics obtained by analyzing the very low-amplitude vibration results obtained from the impulse hammer tests, a sine sweep test campaign was also independently conducted using a eccentric mass shaker mounted at the top of the concrete roof. The roof shaker was used to excite the structure and compute the modal frequencies from the power spectral densities of the recorded acceleration signals. Complete frequency sweeps from 1 to 50 Hz with increasing step of 0.1 Hz were carried out. The low vibration levels that resulted from these tests were significantly higher than the vibration tests resulted from the impulse hammer tests. In contrast to the impulse hammer series of 6 tests lasting a couple of minutes after each earthquake event, each sine sweep test lasted a period of half an hour. Such experiments were performed only for the initial un-reinforced structure and yielded the same natural frequencies as the impulse hammer tests. Thus, it was not deemed necessary to perform these time-consuming sine sweep experiments for the reinforced masonry structure.

The recorded acceleration time histories and the impulse force for each test were used to obtain the frequency response functions and then the PolyMAX frequency domain method (Peeters *et al.* 2004) was applied to identify the modal characteristics of the structure. For this, the modal identification, graphical user interface, toolbox MI-Tool developed in the Structural Dynamics Laboratory of the University of Thessaly (Ntotsios 2009) was conveniently used to estimate the modes. The identified modal frequencies and modal damping ratios for the lowest four modes are reported in Figs. 9 and 10, respectively, as a function of the seismic event for both the un-reinforced and the reinforced building. For each seismic event, more than one modal frequencies may be shown that results from the analysis of multiple vibration tests available. Representative mode shapes identified by the measurements are shown in Fig. 11 and should be compared to the mode shapes in Fig. 12 predicted by the nominal finite element model developed in Section 2.3. The length of the arrows in Fig. 11 denotes the magnitude of each component of the mode shape along the measured DOF. It is clear that the first lowest mode in Fig. 11(a) corresponds to the first shear mode in the horizontal  $y$ -direction perpendicular to the direction of the shake table motion, the second lowest mode in Fig. 11(b) corresponds to the first shear mode in the horizontal  $x$  direction which is along the direction of the shake table motion, the third mode in Fig. 11(c) is dominated by the first bending mode (out-of-plane mode) of

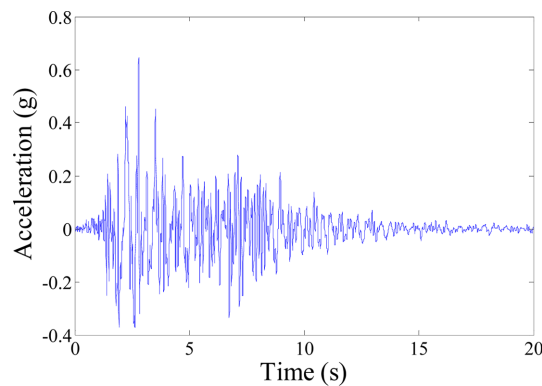


Fig. 8 2009 W-E component of L' Aquila earthquake shaking



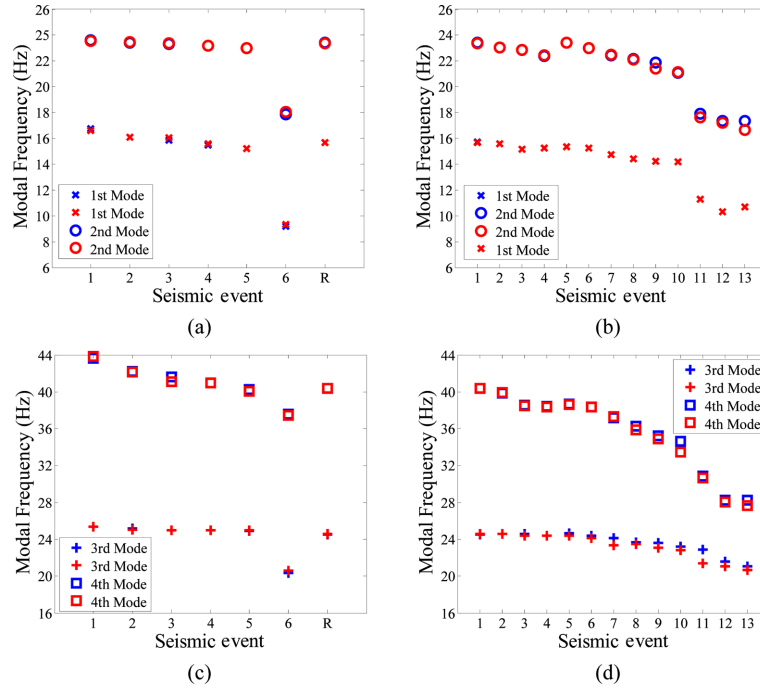


Fig. 9 Evolution of modal frequencies as a function of the seismic events (a),(c) un-reinforced building, (b),(d) reinforced building

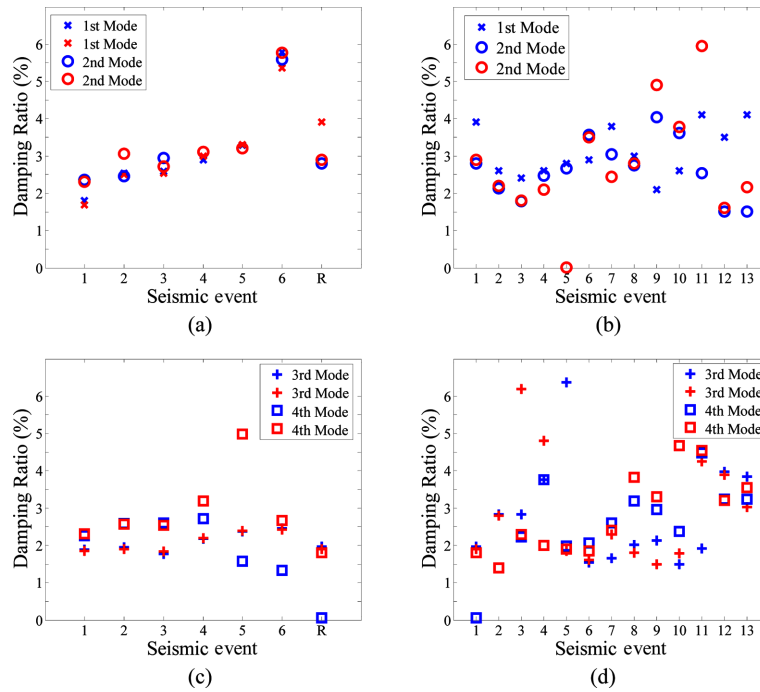


Fig. 10 Evolution of modal damping ratios as a function of the seismic events (a) and (c) un-reinforced building, (b) and (d) reinforced building



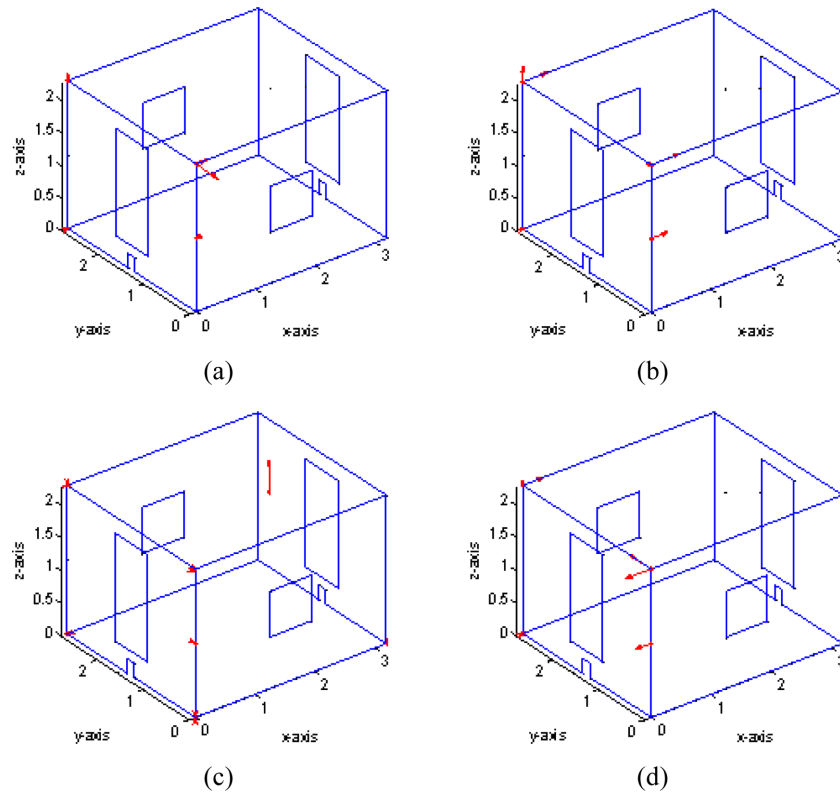


Fig. 11 Identified mode shapes (a) first mode, (b) second mode, (c) third mode and (d) fourth mode

the concrete roof, while the fourth mode in Fig. 11(d) corresponds to a torsional mode of the building that arise from the rotation of the roof with respect to the vertical  $z$ -direction.

In addition to the acceleration measurements, FBG sensors data were recorded during the seismic events and the subsequent low-amplitude vibration tests of the reinforced building, with the exception of test number 5. FBG sensors time histories were then used to identify the modal characteristic of the structure, to be compared with the results obtained by the accelerometers time histories. FBG data, recorded at 685 Hz, were re-sampled at 100 Hz. Then filtering was applied to remove low frequencies from 0 to 0.5 Hz which results in noise modes. This noise, confirmed from the experimental/laboratory tests on the FBG sensors installed on the building, is due to the stiffness on the connection masonry/FRP which induced the noise at very low frequencies. Finally the measurements were processed to identify the modal frequencies and the damping ratios. The Eigensystem Realization Algorithms (ERA) as proposed by (Juang and Pappa 1985) was adopted for the modal identification purpose. From FBG sensors results, the identified modal frequencies, as a function of the seismic event for the reinforced building, are reported in Fig. 13 with reference to the lowest four modes, while in Fig. 14 the identified modal damping ratios are reported.

With reference to Fig. 13, strong analogies can be highlighted in comparison to the results as calculated from acceleration measurements in Fig. 9. This is particularly evident for the 1<sup>st</sup> and the 2<sup>nd</sup> mode, while for the 3<sup>rd</sup> and the 4<sup>th</sup> mode more inconsistencies are shown. However it is interesting to note that the FBG estimated modal frequencies for the 1<sup>st</sup> and the 2<sup>nd</sup> mode are particularly close to the ones estimated from accelerometers for the last three seismic tests, which resulted in inducing

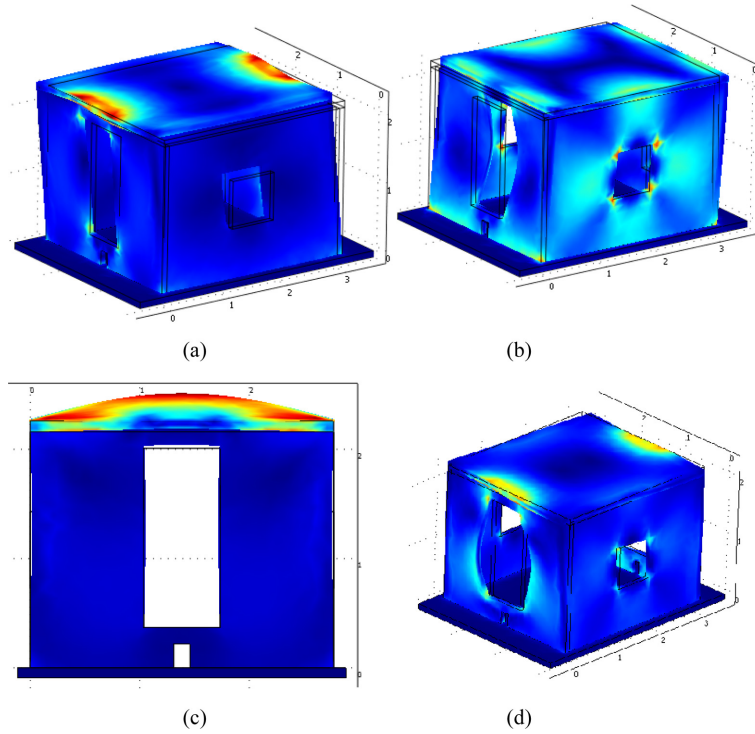


Fig. 12 Finite element model predicted mode shapes (a) first mode, (b) second mode, (c) third mode and (d) fourth mode

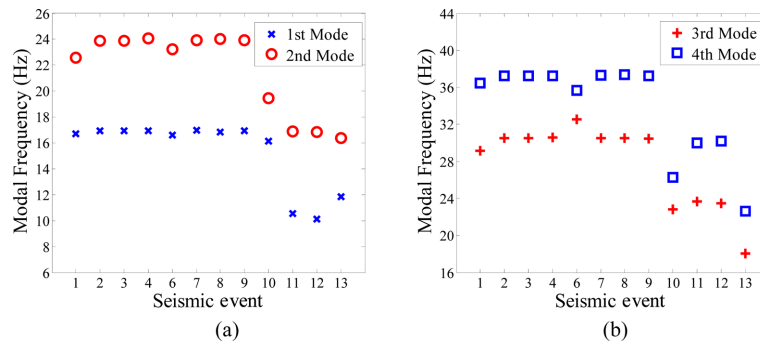


Fig. 13 Evolution of modal frequencies as a function of the seismic events for the reinforced building using FBG sensors

the most significant changes to the modal characteristic of the reinforced building. This can be assessed by looking at Fig. 15, which reports the ratio of the modal frequencies estimated from accelerations and FBG measurements.

On the contrary from the results in Fig. 13(b), it can be noted that the 3<sup>rd</sup> and the 4<sup>th</sup> modal frequency trends as calculated from FBG sensors data present some differences with respect to the modal frequency trend estimated from acceleration data. For the 3<sup>rd</sup> mode dominated by the out of plane motion of the roof (see Fig. 12(c)), this can be explained from the high noise-to-signal ratio contained at the masonry wall mounted FBG sensors at the frequency range of the 3<sup>rd</sup> mode since

the main strain motion of the roof is not measured directly by the FBG sensors. For the 4<sup>th</sup> mode, these differences could be explained by the fact that this mode is torsional, and that, even if cross-correlations are implemented when processing the data, torsion modes might not be clearly detected by the longitudinal FBG sensors.

## 5.2 Correlation of dynamic characteristics with seismic intensity, building damage and retrofitting actions

The change (reduction or increase) of the lowest four modal frequencies observed in Fig. 9 and in Fig. 13 is due to the change in stiffness of the masonry building caused by damage under the applications of the seismic events or by the retrofitting actions. The results in these figures confirm that the identified values of the modal frequencies are highly dependent on the intensity levels of the seismic events and the corresponding health state of the building. To further illustrate this the PGAs of the seismic events are shown as a functions of the seismic events in Figs. 16(a) and (b) for the un-reinforced and the reinforced building, respectively.

With respect to the PGAs evolution with the seismic tests, the feasibility of the FBG sensors in detecting the changes of the dynamic characteristics and propagation of damage can also be assessed. This can be investigated by looking at Fig. 17 which shows the evolution of the standard deviation of the strain data recorded by the S8 horizontal FBG sensors located close to the base as

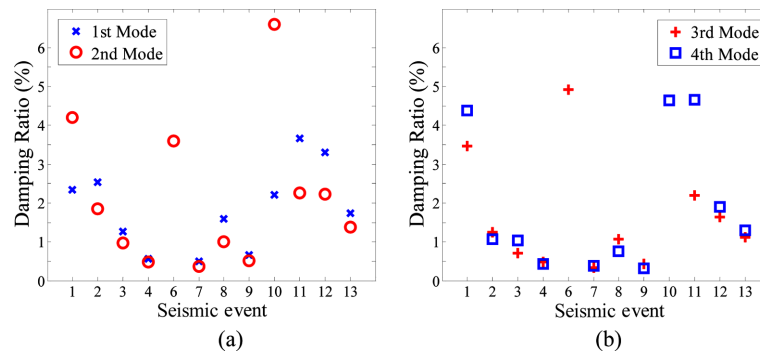


Fig. 14 Evolution of modal damping ratios as a function of the seismic events for the reinforced building using FBG sensors

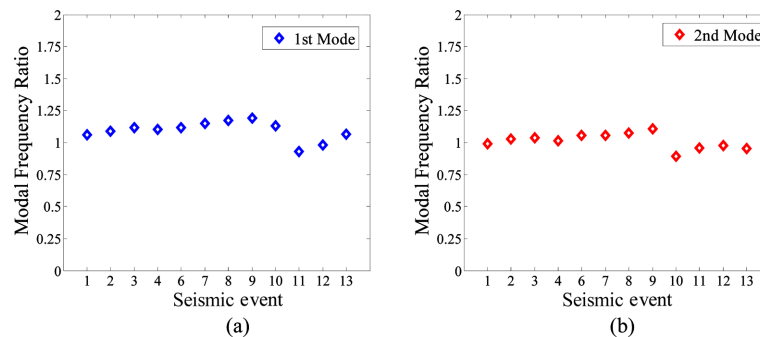


Fig. 15 Ratio of the modal frequencies values for the reinforced building among the FBG and accelerometers, (a) 1<sup>st</sup> mode and (b) 2<sup>nd</sup> mode

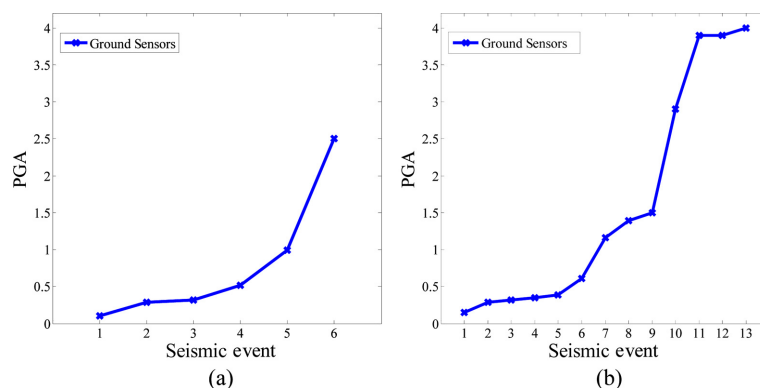


Fig. 16 Evolution of PGA as a function of the seismic events (a) un-reinforced building and (b) reinforced building

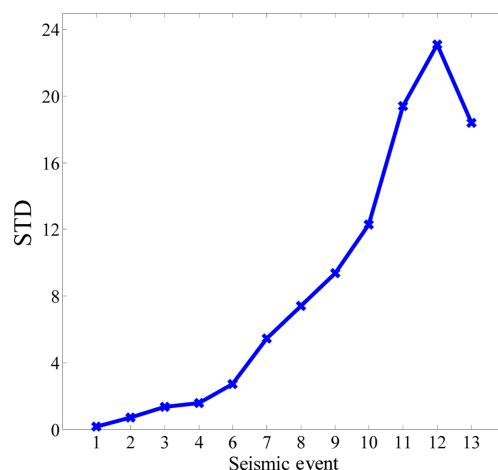


Fig. 17 Evolution of the standard deviation of strain recorded by the FBG sensors as a function of the seismic events for the reinforced building

shown in Fig. 3(a), during the seismic tests for the reinforced building. The trend depicted in Fig. 17 is very close to that showed in Fig. 16(b). The evolution of the PGAs and of the standard deviation of FBG sensors strain measurements with the seismic tests is very close.

From the results in Figs. 9(a) and (c), one clearly observes that earthquake shaking damages internally the structure causing a stiffness degradation, manifested as a reduction in the values of the modal frequencies. As the intensity of the earthquake event increases the values of all four modal frequencies reduce. However, for the first five seismic events no visible cracking in the masonry walls was evident for the case of the un-reinforced masonry structure. The small reduction of the modal frequencies observed is an indication of internal damage caused by non-visible micro cracking in the mortar and the interface between the mortar and the bricks. A large reduction in the modal frequency is observed after the sixth earthquake event which is due to significant stiffness deterioration caused by the severe damage in the masonry walls. As mentioned before, under the action of the sixth seismic event all four masonry walls sustained large crack openings, shown in Fig. 6.

After the building was repaired and reinforced with the GFRP strips, the identified modal frequencies of the retrofitted structure shown as the reinforcement event “R” in Figs. 9(a) and (c) have increased substantially to almost the initial values of the modal frequencies of the un-reinforced building at its original un-damaged state. Thus the strengthening resulted in recovering the original stiffness levels of the un-reinforced building.

Based on the results obtained in Figs. 9(b) and (d) and Figs. 13(a), and (b) for the re-tested reinforced masonry building, a similar reduction in the modal frequency values is observed as the intensity of the seismic events increases. The first ten seismic events reduced slightly the modal frequencies, while the last three strong seismic events reduced the modal frequencies considerably. However, no visible cracking in the reinforced masonry walls was evident for all earthquake tests for the case of reinforced masonry structure. The reduction in modal frequencies is again due to stiffness degradation and it is an indication of internal damage caused by micro cracking in the mortar and the interface between the mortar and the bricks, as well as possible delamination between GFRP strips and the masonry walls. Such reduction was also observed for the first five seismic events for the un-reinforced building and it seems to indicate that the same damage mechanism was triggered even for the reinforced structure. This is consistent with similar results observed by Benedetti *et al.* (2001).

The aforementioned results provide clear evidence that the changes in modal frequency are correlated with (a) stiffness degradation in the structure caused by damage after a seismic event, or (b) stiffness improvement caused by the retrofitting and strengthening actions using GFRP strips. This evolution (reduction or increase) of the modal frequencies can be used as a damage or strengthening index indicator. In addition, the availability of the modal frequency values of the undamaged building is useful for stiffness restoration of the damaged building using repair and strengthening actions. When the modal frequencies of a building are available using vibration measurements before a damaging event, then the restoration steps for a damaged building can be continued up to the level where the modal frequencies of the retrofitted structure reach (or even exceed) the original values of the undamaged building. This is a safe, validated procedure confirming that the initial stiffness of the structure is restored. However, if the modal frequencies of the undamaged building are not known and the building is damaged after an earthquake, the level of repairing cannot be defined with sufficient precision. Numerically predicted modal frequencies of the undamaged building based only on simplified finite element models for masonry walls, provide only qualitative information and not accurate quantitative information about the actual dynamic characteristic of the building. To provide a more accurate quantitative prediction of the building dynamic properties, numerical models should be developed that properly take into account the highly complex composite nature of the masonry walls, as well as the boundary conditions resulting from the presence of window and door openings, the connections of the walls at the corners as well as the connections of the walls with the table and the roof.

Based on the results in Figs. 10 and 14, the damping ratios of the lowest four modes at low vibration levels under which the post-earthquake vibration tests were conducted range from 1% to 6% based on the information extracted by the acceleration sensors, while for the seismic events 4 to 9 it falls below 1% to values as low as 0.2% based on information extracted from the FBG sensors. The damping ratio values estimated from the acceleration sensors for the lowest three modes of the un-reinforced building tend to increase with the intensity of the seismic event. This indicates that damage causes the damping ratios of the structure to increase in general. The overall increase of damping ratios with damage is consistent with results reported for other structures. However, a certain increasing tendency is not clear for the reinforced building. An increased tendency with the

intensity of the seismic event is observed for the 1<sup>st</sup> and the 4<sup>th</sup> mode in Figs. 10(b) and (c). This tendency is not observed for the 2<sup>nd</sup> mode in Fig. 10(b). The 3<sup>rd</sup> and the 4<sup>th</sup> mode show a significant increase in the damping values for the last four seismic events (events 10 to 13) which were significantly stronger as observed by the PGA values in Fig. 16(b). Similar higher values of the damping ratios are also observed in Fig. 14 for the last four seismic events (events 10 to 13) for all modes identified from the FBG sensors. The use of the evolution of the damping ratio values as a damage index indicator is not suitable partly due to the fact that the fluctuation in the estimates of the modal damping ratios from repeated vibration tests using experimental modal analysis techniques is relatively high and this fluctuation may mask the real correlation that may exist between the modal damping ratios and the damage or strengthening actions on the structure.

Concluding, progressively increasing the intensity of the seismic event has an effect on the stiffness of the un-reinforced and reinforced structure as it is observed by the reduction in the modal frequencies. The un-reinforced brittle masonry walls suffered severe damage, losing structural integrity and posing increasing threat to occupants. The GFRP strips used to retrofit the damaged structure maintained the integrity of the structure, causing no visible damage.

## 6. Conclusions

A series of progressively intensified shake table seismic tests were performed on an un-reinforced and subsequently reinforced and re-tested full-scale masonry structure in order to evaluate its seismic vulnerability and to validate the effectiveness of the reinforcement to withstand earthquakes. Low amplitude vibration tests were carried out to monitor the evolution of the dynamic characteristics of the structure after each seismic test. The un-reinforced masonry building was severely damaged with large visible crack openings manifested at all masonry walls. The retrofitted masonry building was obtained from the severely damaged un-reinforced masonry building by fixing the cracked masonry walls and bonding on the masonry walls specially designed GFRP bands. Despite the larger amplitude earthquake events applied on the reinforced building, no visible cracks were observed. The GFRP material, covering 20% of the masonry wall surfaces, was proven to be very effective in reinforcing the masonry building to withstand earthquake events significantly larger in magnitude than the ones caused severe damage to the un-reinforced building.

It was demonstrated that changes in modal frequency are correlated with stiffness degradation caused by minor to severe damage in the masonry walls after a seismic event, as well as correlated with stiffness improvement caused by repair and GFRP strip strengthening actions. The reduction or increase of the modal frequencies identified from low-amplitude vibration tests can be respectively used as damage or strengthening index indicators. Severe damage due to large crack formations along the un-reinforced masonry walls, is associated with significant stiffness reduction manifested as substantial shift in the lowest four modal frequency values, especially for the mode with the dominant deflections in the direction of shaking. Repair and strengthening with GFRP strips can restore and even exceed the stiffness to the original values of the un-damaged un-reinforced structure. The identified modal frequency reductions of the reinforced building under the series of earthquake tests were of similar level as the un-reinforced building. The observed reductions in modal frequencies of the reinforced masonry structure are attributed to the formation of non-visible micro-cracks between the brick and the mortar material which affected the stiffness of the masonry walls and thus the building's global dynamic characteristics. The damping ratios of the lowest four modes

identified from low amplitude vibration tests also show a general increasing tendency with the intensity of seismic excitation and the level of damage. However, such tendency may be hidden by the large fluctuations in the identified values of the modal damping ratios.

This study also investigated the feasibility of FBG sensors embedded into the textile reinforcement as sensors for detecting the changes in the dynamic characteristics of the building and eventually the progression of damage states. It has been demonstrated that the FBG sensors, installed during the seismic tests of the reinforced building, can identify the dynamics of the building at least for in-plane horizontal modes.

The shift of identified modal (resonant) frequencies with the intensity of excitation using low-amplitude vibration tests allows the assessment of the stiffness degradation after each loading event or stiffness improvement after a strengthening event. This procedure seems sufficient for developing a vibration-based damage or repairing assessment technique.

It was experimentally demonstrated that the reinforcement based on the proposed GFRP material strips architecture significantly increases stiffness and strengthens the structure. The proposed reinforcement applied before or after a damaging seismic event can greatly reduce the vulnerability and seismic risk of brick masonry structures. In the future, high strength polymeric fibres may increase further the fibre-matrix capability to absorb energy and also optimize the synergistic interaction between wall and reinforcement.

## Acknowledgements

The partial funding support of the European Project NMP2-CT-2006-026789 (POLYTECT project) is gratefully acknowledged.

## References

- Agarwal, P. and Thakkar, S.K. (2004), "A comparative study of strengthening and retrofitting measures for unreinforced brick masonry model under cyclic testing", *J. Earthq. Eng.*, **8**, 839-863.
- Albert, M.L., Elwi, A.E. and Cheng, J.J.R. (2001), "Strengthening of unreinforced masonry walls using FRPs", *J. Compos. Constr.*, **5**(2), 76-84.
- Bastianini, F., Corradi, M., Borri, A. and Tommaso, A.D. (2005), "Retrofit and monitoring of an historical building using 'smart' CFRP with embedded fibre optic Brillouin sensors", *Constr. Build. Mater.*, **19**, 525-535.
- Benedetti, D., Curydis, P. and Limongelli, P. (2001), "Evaluation of the seismic response of masonry buildings based on energy functions", *Earthq. Eng. Struct. D.*, **30**(7), 1061-1081.
- Beni, F., Lagomarsino, S., Marazzi, F., Magonette, G. and Podestà, S. (2003), "Structural monitoring through dynamic identification", *Proceedings of the 3rd World Conf. on Structural Control*, Wiley, Chichester, U.K.
- Casciati, S. and Faravelli, L. (2010), "Vulnerability assessment for medieval civil towers", *Struct. Infrastruct. E.*, **6**(1-2), 193-203.
- Casciati, S. (2010), "Response surface models to detect and localize distributed cracks in a complex continuum", *J. Eng. Mech. - ASCE*, **136**(9), 1131-1142.
- Casciati, S. and Hamdaoui, K. (2008), "Experimental and numerical studies toward the implementation of shape memory alloy ties in masonry structures", *Smart Struct. Syst.*, **4**(2), 153-169.
- Casciati, S. and Al-Saleh, R. (2010), "Dynamic behavior of a masonry civic belfry under operational conditions", *ACTA Mech.*, **215**(1-4), 211-224.
- CNR-DT 200 (2004), *Guide for the design and construction of externally bonded FRP systems for strengthening existing structures*, National Research Council, Rome, July.

- COMSOL AB (2005), *COMSOL Multiphysics User's Guide*, (<http://www.comsol.com/>).
- Fam, A., Musiker, D., Kowalsky, M. and Rizkalla, S. (2002), "In-plane testing of damaged masonry wall repaired with FRP", *Adv. Compos. Lett.*, **11**(6), 275-281.
- Juang J.N. and Pappa, R.S. (1985), "An eigensystem realization algorithm for modal parameter identification and model reduction", *J. Guid. Control. Dynam.*, **8**(5), 620-627.
- Kiss, R.M., Kollar, L.P., Jai, J. and Krawinkler, H. (2002a), "Masonry strengthened with FRP subjected to combined bending and compression. Part II: Test results and model predictions", *J. Compos. Mater.*, **36**(9), 1049-1063.
- Kiss, R.M., Kollar, L.P., Jai, J. and Krawinkler, H. (2002b), "FRP strengthened masonry beams. Part I: Model", *J. Compos. Mater.*, **36**(5), 521-536.
- Liu, J., Liu, M. and Song, Y. (2007), "Experimental investigation on flexural performance of masonry walls reinforced with GFRP", *J. Wuhan Univ. Technol.*, **22**, 82-84.
- Marcari, G., Manfredi, G., Prota, A. and Pecce, M. (2007), "In-plane shear performance of masonry panels strengthened with FRP", *Compos. Part B – Eng.*, **38**(7-8), 887-901.
- Messervey, T.B., Zangani, D. and Fuggini, C. (2010), "Sensor-embedded textiles for the reinforcement, dynamic characterisation, and structural health monitoring of masonry structures", *Proceedings of the 5th EWSHM 2010*, Sorrento, Italy, June.
- Mosallam, A.S. (2007), "Out-of-plane flexural behavior of unreinforced red brick walls strengthened with FRP composites", *Compos. Part B – Eng.*, **38**(5-6), 559-574.
- Ntotsios, E. (2009), *Modal identification of structures using ambient vibrations: Theory, software and applications*, MSc Thesis, University of Thessaly, Department of Mechanical Engineering, Greece.
- Paquette, J., Bruneau, M. and Brzev, S. (2004), "Seismic testing of repaired unreinforced masonry building having flexible diaphragm", *J. Struct. Eng. - ASCE*, **130**(10), 1487-1496.
- Peeters, B., Van der Auweraer, H., Guillaume, P. and Leuridan, J. (2004), "The PolyMAX frequency-domain method: A new standard for modal parameter estimation?", *Shock Vib.*, **11**(3-4), 395-409.
- Salerno, G. and de Felice, G. (2009), "Continuum modeling of periodic brickwork", *Int. J. Solid. Struct.*, **46**(5), 1251-1267.
- Stefanou, I., Sulem, J. and Vardoulakis I. (2008), "Three-dimensional Cosserat homogenization of masonry structures: elasticity", *ACTA Geotech.*, **3**(1), 71-83.
- Tan, K.H., Patoary, M.K.H. and Roger, C.S.K. (2003), "Anchorage systems for masonry walls strengthened with FRP composite laminates", *J. Reinf. Plast. Comp.*, **22**(15), 1353-1371.
- Triantafillou, T.C. (1998), "Strengthening of masonry structures using epoxy-bonded FRP laminates", *J. Compos. Constr.*, **2**, 96-104.
- Turek, M., Ventura, C.E. and Kuan, S. (2007), "In-plane shake-table testing of GFRP-strengthened concrete masonry walls", *Earthq. Spectra*, **23**(1), 223-237.
- Wight, G.D., Kowalsky, M.J. and Ingham, J.M. (2007), "Shake table testing of post-tensioned concrete masonry walls with openings", *J. Struct. Eng. - ASCE*, **133**(11), 1551-1559.